Adsorption in a nonsymmetric wedge

P. Jakubczyk and M. Napiórkowski
Instytut Fizyki Teoretycznej, Uniwersytet Warszawski, Hoża 69, 00-681 Warszawa, Poland
(Received 19 June 2002; published 17 October 2002)

We study adsorption in a nonsymmetric wedge consisting of two chemically different, homogeneous planes. First, we macroscopically analyze configurations of nonvolatile liquid drop placed in such a two-dimensional wedge and construct phase diagrams describing transitions between various interfacial shapes. Then adsorption is discussed within MFT based on the effective interfacial Hamiltonian. Two regimes for the system parameters — the wedge opening angle (2ϕ) and the critical wetting temperatures of each of the planar walls (T_{W1} and T_{W2}, $T_{W2}<T_{W1}$) — are identified. In one of them we find the critical filling transition at $T_F<T_{W2}$ and the corresponding critical indices which are equal to those found for a symmetric wedge. In the other regime ($T_{W2}<T_F<T_{W1}$) interfacial configurations are similar to those exhibited in the case of a planar substrate consisting of two chemically different parts. In the borderline case ($T_F=T_{W2}$), the interface profile above the wall with the lower wetting temperature becomes parallel to it. The line tensions corresponding to $T_F<T_{W2}$ and $T_F=T_{W2}$ cases are evaluated and the critical exponents — different in each case — are identified. An effective one-dimensional Hamiltonian describing fluctuations along the wedge is constructed for the $T_F<T_{W2}$ case.

DOI: 10.1103/PhysRevE.66.041107 PACS number(s): 68.08.Bc, 68.15.+e, 64.10.+h

I. INTRODUCTION

Numerous recent studies attempt to investigate the influence that a nonplanar substrate's geometry [1–17] or its chemical inhomogeneities [18–29] have on wetting properties. Each of these factors may independently modify the adsorption properties (e.g., the wetting temperature T_W) of the reference system in which the substrate is planar and chemically homogeneous. However, in many experimental situations these two factors are present simultaneously (see Refs. [30–33]). In this paper we take into account both of them by considering a wedge consisting of two chemically different, homogeneous, planar walls. As shown recently for the symmetric case [1,5], at liquid-vapor coexistence and at a temperature $T_F<T_W$ the height of the liquid meniscus at the center of the wedge becomes macroscopically large, while the planar walls of the wedge far from its center remain nonwet. The temperature T_F of the filling transition depends on the wedge opening angle 2ϕ. However, if the walls have different critical wetting temperatures — denoted by T_{W1} for the left wall and T_{W2} for the right wall, $T_{W1}>T_{W2}$ — then it may happen that the critical filling temperature increases up to the right wall wetting temperature T_{W2} and even exeeds it. Actually, the borderline case $T_F=T_{W2}$ turns out to be very interesting because it comprises both the filling and the planar wall wetting aspects of the adsorption.

Section II contains a preliminary thermodynamic analysis of liquid-vapor interfacial configurations under the constraint of constant liquid volume. The corresponding phase diagram parametrized by two contact angles is constructed.

In Sec. III the constraint of constant liquid volume is relaxed and the effective interface model describing adsorption in a nonsymmetric wedge is studied within the mean-field approach. The interfacial morphology is discussed, the corresponding line tension expressions are derived, and their critical properties are evaluated.

In Sec. IV we go beyond the mean-field theory and construct phenomenologically a reduced, one-dimensional Hamiltonian — similar to that proposed by Parry *et al.* [9] — describing fluctuations along the wedge. We point out the difficulties related to this approach in the $T_F=T_{W2}$ case.

Section V contains a summary of the results.

II. THERMODYNAMIC APPROACH

We consider a two-dimensional nonsymmetric wedge consisting of two chemically different, infinite, homogeneous walls, see Fig. 1. The thermodynamic state of the nonvolatile liquid drop is located at the bulk liquid-vapor coexistence, with temperature T below the lower wetting temperature of the two substrates, i.e., $T<T_{W2}$. The equilibrium contact angles formed by the liquid-vapor interface and the walls are uniquely determined by the corresponding Young equations,

$$\cos\theta_i=\frac{\sigma_{gw_i}-\sigma_{lw_i}}{\sigma_{lg}}, \tag{1}$$

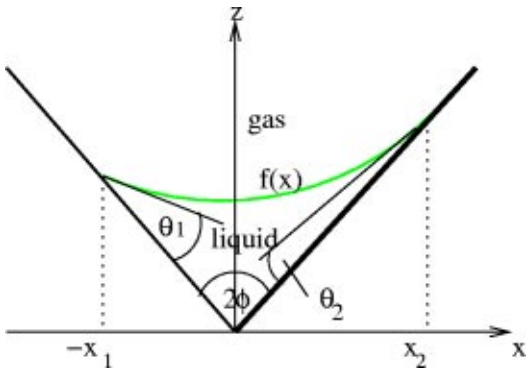

FIG. 1. An example of a meniscus in a nonsymmetric wedge. The shape of the interface is described by the function $f(x)$, which intersects the walls at $x=-x_1$ and $x=x_2$ with contact angles θ_1 and θ_2.

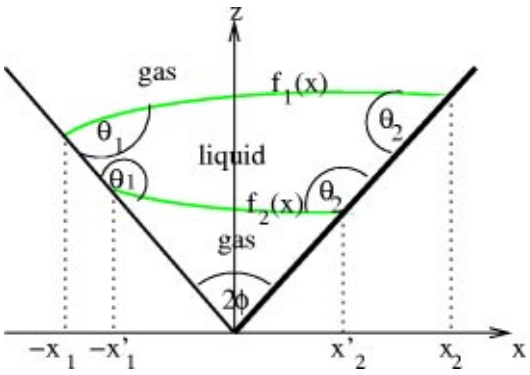

FIG. 2. An example of a bridgelike configuration in a nonsymmetric wedge. We assume $x_i > x_i'$ for $i=1,2$.

where $i=1,2$. The symbols σ_{lg}, σ_{gw_i}, and σ_{lw_i} denote the liquid-vapor, vapor-wall, and liquid-wall surface tensions, respectively. The actual configuration of the liquid-vapor interface is described by the function $f(x)$, see Fig. 1. Its equilibrium shape minimizes the excess surface free-energy functional.

$$\Delta F[f]=\sigma_{lg}\int_{-x_1}^{x_2} dx\left[\sqrt{1+(\partial_x f)^2}-\frac{\cos\theta_1}{\sin\phi}\Theta(-x)-\frac{\cos\theta_2}{\sin\phi}\Theta(x)\right], \tag{2}$$

where $\Theta(x)$ denotes the Heaviside step function and the excess free energy is calculated with respect to the configuration in which the wedge is filled by vapor only. The above functional is minimized under the constraint of a prescribed liquid volume V,

$$\int_{-x_1}^{x_2}[f(x)-|x|\cot\phi]dx=V. \tag{3}$$

Applying the standard Lagrange multiplier method, we are led to the Euler-Lagrange equation, which upon integration gives the equilibrium meniscus shape $\overline{f(x)}$; it forms a part of a circle.

Equations (2) and (3) are valid if the liquid-vapor interface can be represented by a single-valued function. It is a straightforward procedure to extend the above analysis and its conclusions to the case in which this condition is not fulfilled. It turns out that also in the remaining cases — which include the bridgelike configurations with two interfaces — the equilibrium shapes always form a part of a circle. It can be convex [34], concave, bridgelike, or can be located on one of the walls. For a bridgelike configuration (see Fig. 2), the free-energy functional is given by

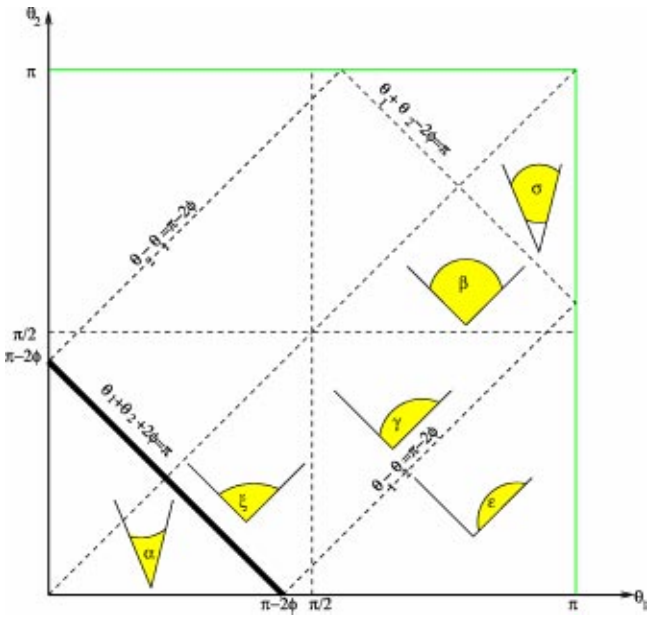

FIG. 3. Phase diagram for a drop of nonvolatile liquid in a nonsymmetric wedge. The schematically sketched configurations refer to the case $\theta_1>\theta_2$; the opposite cases are not displayed for reasons of clarity. Upon crossing the straight line $\theta_1+\theta_2+2\phi=\pi$, the excess free energy changes its sign, which — after relaxing the prescribed volume constraint — gives the locus of filling transitions. For $\theta_1+\theta_2-2\phi>\pi$ there are bridge configurations, while for $|\theta_1-\theta_2|>\pi-2\phi$ the drop is situated on one of the walls. The greek letters enumerate the different drop configurations and refer to the free-energy formulas included in the Appendix. The $\theta_1=\pi/2$ and $\theta_2=\pi/2$ lines denote nothing but validity ranges of certain ΔF expressions (see the Appendix).

$$\Delta F[f_1,f_2]=\sigma_{lg}\left(\int_{-x_1}^{x_2} dx\sqrt{1+(\partial_x f_1)^2}+\int_{-x_1'}^{x_2'} dx\sqrt{1+(\partial_x f_2)^2}-\sum_i \frac{x_i-x_i'}{\sin\phi}\cos\theta_i\right). \tag{4}$$

After inserting the profiles determined above into the free-energy functional and selecting — for each value of system parameters θ_1, θ_2, and ϕ — the absolute minimum, one obtains the respective free energy. In different ranges of the system parameters the corresponding expressions for the free energy take different forms because the geometrical problem leading to them is slightly different in each range. They are displayed in the Appendix. The conclusions are presented in Fig. 3.

We pointout that the condition $|\theta_1-\theta_2|+2\phi>\pi$ implies that a drop placed on one of the substrates corresponds to the only possible interfacial configuration.

For concave interfaces one has $\Delta F<0$, while for all other configurations $\Delta F>0$. The bridgelike configuration is possible, provided the condition $\theta_1+\theta_2-2\phi>\pi$ is fulfilled. In this case the bridge is energetically favored over the convex meniscus and a drop sitting on one wall. All configurations with more than two interfaces are energetically disfavored.

We note that in all the derived expressions for ΔF, the excess free energy is proportional to $\sqrt{V}$. For $\theta_1+\theta_2+2\phi<\pi$ — which corresponds to $\Delta F<0$ — the excess free energy decreases upon increasing V, unlike in all the situations when $\Delta F>0$ and it increases with V. Thus we conclude that when the constant volume constraint is relaxed, V will either grow to infinity or decrease to 0. The condition

$$\theta_1+\theta_2+2\phi=\pi \tag{5}$$

marks the filling transition. It reduces to the well known result (see Refs. [1,5]) that the filling transition in the symmetric wedge takes place at $\theta=\pi/2-\phi$.

We also note the change in the interfacial morphology for $|\theta_1-\theta_2|=\pi-2\phi$ at which a single drop sitting on one wall becomes stable. In the following section we show how both these transitions manifest themselves within the mesoscopic description of adsorption in the wedge.

III. ADSORPTION IN NONSYMMETRIC WEDGE

Adsorption in a three-dimensional wedge will be described within the mean-field approach based on the effective interfacial Hamiltonian. Since the wedge is translationally invariant along its edge, i.e., in the y direction, the mean-field solution for the equilibrium interfacial profile displays this symmetry and depends only on x. Thus, effectively the mean-field solutions correspond to a two-dimensional problem discussed in the preceding section, but now the fixed volume constraint is relaxed. The phenomenological effective interfacial Hamiltonian $\mathcal{H}[f(x)]$ has the following form:

$$\mathcal{H}[f(x)]=\int_{-\infty}^{0}dx\left\{\frac{\sigma_{lg}}{2}\left[\left(\frac{df}{dx}\right)^2-\alpha^2\right]+[V_1(l(x))-V_1(l_{\pi_1})]\right\}+\int_0^{\infty}dx\left\{\frac{\sigma_{lg}}{2}\left[\left(\frac{df}{dx}\right)^2-\alpha^2\right]+[V_2(l(x))-V_2(l_{\pi_2})]\right\}, \tag{6}$$

where $V_{1,2}$ are the effective inteface potentials corresponding to the planar walls forming the substrate. They are chosen is such a way that each wall separately undergoes critical wetting at the corresponding temperature T_{Wi}, $i=1,2$. The potentials $V_{1,2}$ depend on the distance between the interface and the substrate, $l(x)=f(x)-|x|\cot\phi$. The symbols l_{π_i}, $i=1,2$, denote the reference equilibrium thickness of the liquid layer adsorbed on a single planar wall of ith type. We stick to the wide-wedge approximation introduced in Ref. [5], in which the interaction of the interface with the nearest wall is taken into account while that with the other wall is neglected. We also assume that the substrates' critical wetting temperatures are close to each other, as the effective interaction model used below is valid for temperatures close to wetting. Accordingly we put $\sin\phi\simeq 1$ and $\cos\phi\simeq\alpha=\pi/2-\phi$. This approximation does not influence qualitatively any of our further conclusions.

Equation (6) can be rewritten in the following form:

$$\mathcal{H}[l]=\int_{-\infty}^{0}dx\left\{\frac{\sigma_{lg}}{2}\left(\frac{dl}{dx}\right)^2+V_1(l(x))-V_1(l_{\pi_1})\right\}+\int_0^{\infty}dx\left\{\frac{\sigma_{lg}}{2}\left(\frac{dl}{dx}\right)^2+V_2(l(x))-V_2(l_{\pi_2})\right\}+\sigma_{lg}\alpha[l_{\pi_2}+l_{\pi_1}-2l(0)]. \tag{7}$$

Within the MFT approximation, the equilibrium meniscus shape $\overline{l}$ minimizes the effective Hamiltonian, which implies the following equation for $\overline{l}$:

$$\frac{\sigma_{lg}}{2}\frac{d}{dx}\left(\frac{d\overline{l}}{dx}\right)^2=\frac{d}{dx}V_{1,2}(\overline{l}), \tag{8}$$

where we take $V_1(\overline{l})$ for $x\leqslant 0$ and $V_2(\overline{l})$ otherwise. The boundary conditions depend on the temperature of the system. More precisely, one has to distinguish the cases of $T-T_{W2}$ being negative (which corresponds to the right wall being nonwet), or positive. Thus we consider two cases.

A. $T\leqslant T_{W2}$

The boundary conditions for this case take the form $\lim_{x\to\mp\infty}\overline{l}=l_{\pi_{1,2}}$. Integrating Eq. (8) one is led to the following equation for $\overline{l}(0)$:

$$8\sigma_{lg}\alpha^2[V_1(\overline{l}(0))-V_1(l_{\pi_1})]=[V_2(\overline{l}(0))-V_1(\overline{l}(0))-V_2(l_{\pi_2})+V_1(l_{\pi_1})-2\sigma_{lg}\alpha^2]^2. \tag{9}$$

From now on we restrict our analysis to the model potential $V_{1,2}$ corresponding to the short-range interactions (see Refs. [4,5,7,35]),

$$V_{1,2}(l)=a\tau_{1,2}\exp\left(-\frac{l}{\xi}\right)+b\exp\left(-\frac{2l}{\xi}\right), \tag{10}$$

where the dimensionless parameters $\tau_i=(T-T_{Wi})/T_C$ measure the temperature with respect to the ith wall wetting temperature, and T_C denotes the bulk critical temperature. As the result one obtains the following expression for $\overline{l}(0)$:

$$\overline{l}(0)=-\xi\ln\left[-\frac{a(\tau_1+\tau_2)}{4b}-\sqrt{\frac{\sigma_{lg}}{2b}}\alpha\right]. \tag{11}$$

The singularity of $\overline{l}(0)$ marks the filling transition, which takes place at

$$T_F=\frac{T_{W1}+T_{W2}}{2}-\alpha\frac{\sqrt{2\sigma_{lg}b}}{a}T_C. \tag{12}$$

Equation (11) can be rewritten as $\overline{l}(0)=-\xi\ln[-(a/2b)(T-T_F/T_C)]$. It is straightforward to check that the condition $T_F<T_{W2}$ corresponds to

$$\alpha>\frac{a}{\sqrt{8\sigma_{lg}b}}\frac{T_{W1}-T_{W2}}{T_C}. \tag{13}$$

This condition is always fulfilled for the symmetric case. We note that in the limiting case $\alpha=(a/\sqrt{8\sigma_{lg}b})[(T_{W1}-T_{W2})/T_C]$, we get $T_F=T_{W2}$ and $\overline{l}(0)=l_{\pi_2}$. The meniscus shape can be found by integrating Eq. (8),

$$\overline{l}(x)=\begin{cases} l_2(x)=\xi\ln\left\{\dfrac{2b}{a\tau_2}\left[\left\{1+\dfrac{a\tau_2}{2b}\exp\left(\dfrac{l(0)}{\xi}\right)\right\}\exp\left(\dfrac{a\tau_2}{\sqrt{2\sigma_{lg}b}}\dfrac{x}{\xi}\right)-1\right]\right\} \\ l_1(x)=\xi\ln\left\{\dfrac{2b}{a\tau_1}\left[\left\{1+\dfrac{a\tau_1}{2b}\exp\left(\dfrac{l(0)}{\xi}\right)\right\}\exp\left(-\dfrac{a\tau_1}{\sqrt{2\sigma_{lg}b}}\dfrac{x}{\xi}\right)-1\right]\right\}, \end{cases} \tag{14}$$

where l_2 corresponds to $x>0$, l_1 to $x<0$. For arbitrary values of the system parameters, $l_1(x)$ is an increasing function of x while $l_2(x)$ decreases, provided the condition in Eq. (13) holds, increases if $\alpha<(a/\sqrt{8\sigma_{lg}b})[(T_{W1}-T_{W2})/T_C]$; and remains constant in the borderline case $\alpha=(a/\sqrt{8\sigma_{lg}b})[(T_{W1}-T_{W2})/T_C]$. For typical interfacial shapes, see Fig. 4.

B. $T>T_{W2}$

In this section we investigate the case $\tau_2>0$ and $\tau_1<0$, which corresponds to $\alpha<(a/\sqrt{8\sigma_{lg}b})[(T_{W1}-T_{W2})/T_C]$. The boundary conditions take the form $\lim_{x\to\infty}\overline{l}(x)=\infty$, $\lim_{x\to-\infty}\overline{l}(x)=l_{\pi_1}$, $\lim_{x\to\infty}d\overline{l}/dx=0$ (we assume that the presence of the left wall does not influence the interface behavior in $+\infty$). After integrating Eq. (8) one obtains

$$T_F=T_{W1}-\alpha\frac{\sqrt{8\sigma b}}{a}T_C, \tag{15}$$

which fulfills the inequality $T_{W2}<T_F<T_{W1}$. The limiting case $T_F=T_{W1}$ can be reached only in the flat substrate limit. The meniscus shape takes the following form:

$$l(x)=\begin{cases} l_2(x)=\xi\ln\left\{\dfrac{1}{a\tau_2}\left[-b+\dfrac{\sigma_{lg}}{2}\left(\dfrac{a\tau_2 x}{\xi\sigma_{lg}}+\sqrt{\dfrac{2}{\sigma_{lg}}(a\tau_2 e^{l(0)/\xi}+b)}\right)\right]\right\} \\ l_1(x)=\xi\ln\left\{\dfrac{2b}{a\tau_1}\left[\left(1+\dfrac{a\tau_1}{2b}\exp\left(\dfrac{l(0)}{\xi}\right)\right)\exp\left(-\dfrac{a\tau_1}{\sqrt{2\sigma_{lg}b}}\dfrac{x}{\xi}\right)-1\right]\right\}, \end{cases} \tag{16}$$

where

$$l(0)=-\xi\ln\left\{\frac{-4\sigma_{lg}a\alpha^2(\tau_2+\tau_1)-\dfrac{a^3}{2b}\tau_1^2(\tau_2-\tau_1)-\sqrt{2\dfrac{\sigma_{lg}}{b}}a\alpha\left(a\tau_1(2\tau_2-\tau_1)+8\sigma_{lg}\dfrac{b}{a}\alpha^2\right)}{2[8\sigma_{lg}b\alpha^2-a^2(\tau_2-\tau_1)^2]}\right\}. \tag{17}$$

The profile $l(x)$ exhibits logarithmic divergence for $x\to\infty$. A corresponding interfacial shape is displayed schematically in Fig. 5.

C. Macroscopic analogies

The relation between the contact angle $\theta_{1,2}$ and the minimum value of the effective interface potential $V(l_{\pi_{1,2}})$ follows from the Young equation

$$V(l_{\pi_{1,2}})=\sigma_{lg}(\cos\theta_{1,2}-1). \tag{18}$$

After expanding both sides of Eq. (18) in powers of $\tau_{1,2}$ we find $\theta_{1,2}=(-a/\sqrt{2\sigma_{lg}b})\tau_{1,2}$. Using the above result, it is straightforward to check that the thermodynamic condition for a convex interface having contact with both walls $\theta_1-\theta_2+2\phi\leqslant\pi$ leads, upon expansion, to the following inequality:

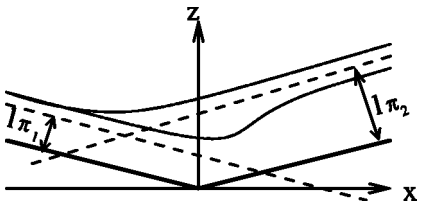

FIG. 4. Schematic configurations of the liquid-vapor interface. The upper curve corresponds to the $T<T_F<T_{W2}$ case, while the lower curve corresponds to the $T_{W1}>T_F>T_{W2}>T$ case. The broken lines denote asymptotes.

$$\cos\phi > \sin\left(\frac{\theta_2-\theta_1}{2}\right)=\frac{a(T_{W1}-T_{W2})}{T_C\sqrt{2\sigma_{lg}b}}+O(\tau_i^2). \quad (19)$$

After neglecting terms quadratic in $\tau_{1,2}$ one obtains the mesoscopic condition for filling temperature T_F staying below T_{W2} [36]. Analogously the condition for the interface being concave, $\theta_1+\theta_2+2\phi\leqslant\pi$, leads to the following inequality:

$$\cos\phi > \sin\frac{\theta_1+\theta_2}{2}=\frac{-a}{\sqrt{2\sigma_{lg}b}}\,\frac{\tau_1+\tau_2}{2}+O(\tau_i^2). \quad (20)$$

In the mesoscopic approach it corresponds to the condition for the wedge being filled.

D. Line tension

The line contribution η to the free energy is obtained by subtracting from the total free energy $\mathcal{H}[\overline{l}]$, the surface energy of the reference configurations described by two asymptotes $A_{1,2}(x)=\mp x\cot\phi+l_{\pi_{1,2}}\simeq\mp\alpha x+l_{\pi_{1,2}}$, which intersect at $x_0=\frac{1}{2}\tan\phi(l_{\pi_1}-l_{\pi_2})\simeq\frac{1}{2}(l_{\pi_1}-l_{\pi_2})$. After changing the integration variables, the line contribution per unit length along the wedge takes the form

$$\begin{aligned}\eta=&\int_{l_{\pi_1}}^{l(0)}dl\{\sqrt{2\sigma_{lg}}\sqrt{V_1(l)-V_1(l_{\pi_1})}-\sigma_{lg}\alpha\}\\&+\int_{l(0)}^{l_{\pi_2}}dl\{\pm\sqrt{2\sigma_{lg}}\sqrt{V_2(l)-V_2(l_{\pi_2})}+\sigma_{lg}\alpha\}\\&-\int_{x_0}^{0}dx[V_1(2x\alpha+l_{\pi_2})-V_1(l_{\pi_1})],\end{aligned} \quad (21)$$

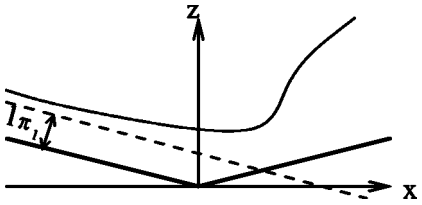

FIG. 5. Schematic configuration of the liquid-vapor interface for $T_F>T>T_{W2}$. The broken line denotes the asymptote.

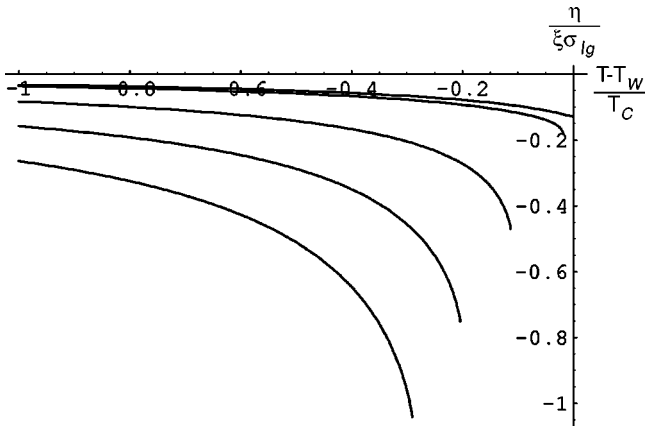

FIG. 6. The dependence of $\eta/\xi\sigma_{lg}$ on temperature for different values of the opening angle ϕ for $T\leqslant T_F\leqslant T_{W2}$. All curves terminate at $T=T_F$, the upper one corresponds to $T_F=T_{W2}$.

where the $+$ sign corresponds to $T_F>T_{W2}$ and vice versa for the $-$ sign. For the effective potential in Eq. (10), one obtains

$$\begin{aligned}\eta=&-2\xi\sigma_{lg}\alpha+\xi\sigma_{lg}\ln\left[\frac{\tau_1+\tau_2}{2\tau_2}+\frac{\sqrt{2\sigma_{lg}b}\,\alpha}{a\tau_2}\right]\left(\alpha+\frac{a\tau_2}{\sqrt{2\sigma_{lg}b}}\right)\\&+\xi\sigma_{lg}\ln\left[\frac{\tau_2+\tau_1}{2\tau_1}+\frac{\sqrt{2\sigma_{lg}b}\,\alpha}{a\tau_1}\right]\left(\alpha+\frac{a\tau_1}{\sqrt{2\sigma_{lg}b}}\right)\\&+\frac{a^2\xi}{16b\alpha}\left(\tau_2^2-4\tau_2\tau_1+3\tau_1^2+2\tau_1^2\ln\frac{\tau_2}{\tau_1}\right).\end{aligned} \quad (22)$$

For $T_F<T_{W2}$ this equation may be written as

$$\eta=\xi\sigma_{lg}\frac{T-T_F}{T_C}\ln\left(\frac{T_F-T}{T_C}\right)+A_1, \quad (23)$$

while for $T_F=T_{W2}$ it takes the form

$$\eta=\frac{\xi\sigma_{lg}a}{\sqrt{8\sigma_{lg}b}(T_{W1}-T_F)T_C}(T-T_F)^2\ln\left(\frac{T_F-T}{T_C}\right)+A_2, \quad (24)$$

where A_1 and A_2 are decreasing, negative functions of temperature, analytic for $T\leqslant T_F$. The dependence of η on temperature for different values of ϕ is shown in Fig. 6.

We remark that the method of evaluating η applied here is unsuitable for the case $T_F>T_{W2}$, which may occur for ϕ large enough. We note that for $\phi\to\pi/2$ the abscissa x_0 of the asymptotes intersection approaches $-\infty$. This behavior corresponds to the right asymptote extending from $-\infty$ to $+\infty$ in the limit of a planar substrate and it certainly lacks physical sense. Bearing this in mind we substracted a reference configuration which is discontinuous at $x_0=0$ (similarly as in Ref. [29] for the planar, inhomogeneous substrate case). Then we find η to diverge logarytmically at $T=T_{W2}$, i.e., $\eta\sim\ln[(T_{W2}-T)/T_C]$.

IV. FLUCTUATIONS

An effective way of describing interfacial fluctuations along a symmetric wedge near the filling transition was developed by Parry *et al.* [9]. It exploits the separation of characteristic length scales in the system determined by the correlation lengths along and across the wedge, denoted by ξ_y and ξ_x, respectively. The fluctuations along the wedge are well characterized by the position of the interface at the center ($x=0$) of the wedge, i.e., $l_0(y)\equiv l(0,y)$. For a fixed value of y, the position of the interface practically does not change upon varying x between the walls. Only when the wall is approached, it makes the interface bend and follow its shape. The phenomenological procedure devised for the symmetric case can be implemented in the nonsymmetric case for $T_F<T_{W2}$ as well. Assuming that for temperatures close to the filling temperature (at which $\theta_1+\theta_2+2\phi=\pi$), a practically flat interface tilted with respect to the (x,y) plane, in accordance with the above contact angle values extending between the walls, leads to the following one-dimensional Hamiltonian:

$$\mathcal{H}[l_0(y)]=\sigma_{lg}\int dy\left\{ l_0(y)\left[\theta_2+\theta_1-2\alpha+\frac{1}{2}\left(\frac{1}{\theta_2}+\frac{1}{\theta_1}\right)\times\left(\frac{dl_0}{dy}\right)^2\right]\right\}. \tag{25}$$

It reduces to the corresponding symmetric wedge result for $\theta_1=\theta_2$. Appropriate rescaling of the variables $y\to Y$ and $l_0(y)\to L(Y)$ in the above Hamiltonian,

$$y=\sigma_{lg}^{-1/2}(\theta_1+\theta_2-2\alpha)^{-3/4}(\theta_1^{-1}+\theta_2^{-1})^{1/4}Y, \tag{26}$$

$$l_0(y)=\sigma_{lg}^{-1/2}(\theta_1+\theta_2-2\alpha)^{-1/4}(\theta_1^{-1}+\theta_2^{-1})^{-1/4}L(Y),$$

leads to its parameter-free form

$$\mathcal{H}[L(Y)]=\int dY L(Y)\left(1+\frac{1}{2}[L'(Y)]^2\right). \tag{27}$$

As the result one obtains the following scaling behavior of the average position of the interface $\langle l_0\rangle$ and the correlation length ξ_y:

$$\langle l_0\rangle\sim(\theta_R+\theta_L-2\alpha)^{-1/4}, \tag{28}$$

$$\xi_y\sim(\theta_R+\theta_L-2\alpha)^{-3/4}, \tag{29}$$

from which the values of the critical indices $\beta_0=\frac{1}{4}$ and $\nu_y=\frac{3}{4}$ follow. These values are the same as in the symmetric case (see Refs. [9,10]). The above form of the one-dimensional Hamiltonian is not suitable for studying the case $T_F=T_{W2}$. On one hand it misses the critical interfacial fluctuations related to wetting point of the right wall, while on the other hand these fluctuations become modified by the presence of the left wall.

V. SUMMARY

We have studied the liquid-vapor interfacial configurations in a nonsymmetric wedge. First, the phase diagram describing the configurations of a nonvolatile liquid drop placed in a two-dimensional nonsymmetric wedge has been constructed and parametrized by the contact angles θ_1 and θ_2 corresponding to each of the walls. In addition to configurations known already from the symmetric wedge studies, e.g., the bridge configurations, one finds ranges of contact angles ($|\theta_1-\theta_2|>\pi-2\phi$) in which the drop is located on one wall only and has no contact with the other wall. Second, after relaxing the constant volume constraint and studying adsorption within the mean-field approach based on the effective interfacial Hamiltonian one identifies two regimes for the parameters in which the system behaves differently. If $\cos\phi>(a/\sqrt{8\sigma_{lg}b})[(T_{W1}-T_{W2})/T_C]$, which corresponds to $T_F<T_{W2}$, the system's behavior is similar to that obtained for a symmetric wedge: at $T=T_F$ we find a filling transition at which the position of the interface located above the edge of the wedge diverges. Within the mean-field theory this divergence is logarithmic ($\beta_0^{MF}=0$), while fluctuations modify this result to $\beta_0=\frac{1}{4}$; the corresponding value of the longitudinal correlation length exponent is $\nu_y=\frac{3}{4}$. The nonanalytic behavior of the line tension η is represented by the term $\eta\sim(T-T_F)\ln[(T_F-T)/T_C]$. In the limiting case, $\cos\phi=(a/\sqrt{8\sigma_{lg}b})[(T_{W1}-T_{W2})/T_C]$, which corresponds to $T_F=T_{W2}$, the nonanalyticity of the mean-field line tension is represented by the term $\eta\sim(T-T_F)^2\ln[(T_F-T)/T_C]$.

APPENDIX

In this appendix we collect the results of the macroscopic analysis of the free energy. The expressions for ΔF_i, $i=\alpha,\beta,\gamma,\xi,\epsilon,\sigma$, correspond to different parameter ranges, which are specified in Fig. 3. These expressions are valid for $\theta_1<\theta_2$. To consider the opposite case, i.e., $\theta_1>\theta_2$, one should swap the contact angles in the formulas. Below, we quote the relevant formulas together with the range of their applicability.

(1) $\theta_1+\theta_2+2\phi<\pi$,

$$\Delta F_\alpha=\sqrt{V}\sigma_{lg}\left[\pi-\theta_1-\theta_2-2\phi-\frac{2\cos\theta_1\cos\theta_2+\cos\theta_1\cos(\theta_1+2\phi)+\cos\theta_2\cos(\theta_2+2\phi)}{\sin 2\phi}\right]\left[\frac{1}{2}\sin(\theta_1+\theta_2+2\phi)+\frac{1}{2}[\cos\theta_1+\cos(\theta_2+2\phi)][\cos\theta_2+\cos(\theta_1+2\phi)]\frac{1}{\sin 2\phi}-\frac{\pi}{2}+\frac{\theta_1+\theta_2}{2}+\phi\right]^{-1/2}. \tag{A1}$$

(2) $\theta_1 > \pi/2, \theta_2 > \pi/2$,

$$\Delta F_\beta = -\Delta F_\alpha . \tag{A2}$$

(3) $\theta_2 < \pi/2, \theta_1 + \theta_2 + 2\phi > \pi$,

$$\Delta F_\gamma = \sigma_{lg}\sqrt{V}\Bigg[\theta_1+\theta_2+2\phi-\pi+\cos\Big(\frac{\theta_1+\theta_2}{2}+\phi\Big) \times\frac{1}{\sin\phi\cos\phi}\Bigg\{\cos\theta_1\cos\Big(\frac{\theta_1-\theta_2}{2}+\phi\Big) +\cos\theta_2\cos\Big(\frac{\theta_2-\theta_1}{2}+\phi\Big)\Bigg\}\Bigg]\Bigg[\frac{\theta_1+\theta_2}{2}+\phi-\frac{\pi}{2} -\frac{1}{2}\sin(\theta_1+\theta_2+2\phi)\frac{\cos\theta_2}{\cos(\theta_1+2\phi)}+2\cos^2\Big(\frac{\theta_1+\theta_2}{2} +\phi\Big)\cos^2\Big(\frac{\theta_2-\theta_1}{2}-\phi\Big)\frac{\cos\theta_1}{\cos(\theta_1+2\phi)}\frac{1}{\sin 2\phi}\Bigg]^{-1/2}. \tag{A3}$$

(4) $\theta_1 < \pi/2, \theta_2 < \pi/2, \theta_1 + \theta_2 + 2\phi > \pi$,

$$\Delta F_\xi = \sigma_{lg}\sqrt{V}\Bigg[\theta_1+\theta_2+2\phi-\pi+\cos\Big(\frac{\theta_1+\theta_2}{2}+\phi\Big) \times\frac{1}{\sin\phi\cos\phi}\Bigg\{\cos\theta_2\cos\Big(\frac{\theta_2-\theta_1}{2}+\phi\Big) +\cos\theta_1\cos\Big(\frac{\theta_1-\theta_2}{2}+\phi\Big)\Bigg\}\Bigg]\Bigg[\frac{\theta_1+\theta_2}{2}+\phi-\frac{\pi}{2} -\frac{1}{2}\sin(\theta_1+\theta_2+2\phi)\frac{\cos\theta_1}{\cos(\theta_2+2\phi)}+2\cos^2\Big(\frac{\theta_1+\theta_2}{2} +\phi\Big)\cos^2\Big(\frac{\theta_2-\theta_1}{2}+\phi\Big)\frac{\cos\theta_2}{\cos(\theta_2+2\phi)}\frac{1}{\sin 2\phi}\Bigg]^{-1/2}. \tag{A4}$$

(5) $\theta_1 - \theta_2 + 2\phi > \pi$,

$$\Delta F_\epsilon = 2\sigma_{lg}\sqrt{V}\Big(\theta_2-\frac{1}{2}\sin 2\theta_2\Big)^{1/2}. \tag{A5}$$

(6) $\theta_1 + \theta_2 - 2\phi > \pi$,

$$\Delta F_\sigma = 2\sigma_{lg}\sqrt{V}\Big[\theta_1+\theta_2-\pi-\frac{1}{2}\sin 2\theta_1-\frac{1}{2}\sin 2\theta_2\Big]^{1/2}. \tag{A6}$$

Note a mistake in Eq. (2.13) in Ref. [5]. The correct form of this equation can be obtained from Eq. (A6) upon putting $\theta_1 = \theta_2$.

[1] E.H. Hauge, Phys. Rev. A **46**, 4994 (1992).
[2] R. Netz and D. Andelman, Phys. Rev. E **55**, 687 (1997).
[3] K. Rejmer, M. Napiórkowski, Z. Phys. B: Condens. Matter **102**, 101 (1997).
[4] P.S. Swain and A.O. Parry, Eur. Phys. J. B **4**, 459 (1998).
[5] K. Rejmer, S. Dietrich, and M. Napiórkowski, Phys. Rev. E **60**, 4027 (1999).
[6] A.O. Parry, C. Rascón, and A.J. Wood, Phys. Rev. Lett. **83**, 5535 (1999).
[7] C. Rascón, A.O. Parry, and A. Sartori, Phys. Rev. E **59**, 5697 (1999).
[8] S. Dietrich, in *New Approaches to Old and New Problems in Liquid State Theory-Inhomogeneities and Phase Separation in Simple, Complex and Quantum Fluids*, Vol. 529 of *NATO Advanced Studies Institute, Messina, Italy, 1998, Series C: Mathematical and Physical Sciences*, edited by C. Caccamo (Kluwer, Dordrecht, 1999).
[9] A.O. Parry, C. Rascón, and A.J. Wood, Phys. Rev. Lett. **85**, 345 (2000).
[10] A. Bednorz and M. Napiórkowski, J. Phys. A, **33**, 353 (2000).
[11] A.O. Parry, A.J. Wood, E. Carlon, and A. Drzewiński, Phys. Rev. Lett. **87**, 196103 (2001).
[12] A.O. Parry, M.J. Greenall, and A.J. Wood, J. Phys.: Condens. Matter **14**, 1169 (2002).
[13] A.O. Parry, A.J. Wood, and C. Rascón, J. Phys.: Condens. Matter **12**, 7671 (2000).
[14] K. Rejmer, M. Napiórkowski, Phys. Rev. E **62**, 588 (2000).
[15] A.O. Parry, A.J. Wood, and C. Rascón, J. Phys.: Condens. Matter **13**, 4591 (2001).
[16] P.G. Wapner and W.P. Hoffman, ACS J. Surf. Coll. **18**, 1225 (2002).
[17] C. Rascón and A.O. Parry, Nature (London) **407**, 986 (2000).
[18] P.S. Swain and R. Lipowsky, ACS J. Surf. Coll. **14**, 6772 (1998).
[19] C. Bauer and S. Dietrich, Phys. Rev. E **60**, 6919 (1999).
[20] C. Bauer and S. Dietrich, Phys. Rev. E **61**, 1664 (2000).
[21] P.S. Swain and R. Lipowsky, Europhys. Lett. **49**, 203 (2000).
[22] R. Lipowsky, Curr. Opin. Colloid Interface Sci. **6**, 40 (2001).
[23] P. Lenz and R. Lipowsky, Phys. Rev. Lett. **80**, 1920 (1998).
[24] P. Lenz and R. Lipowsky, Eur. Phys. J. E **1**, 249 (2000).
[25] P. Lenz, W. Fenzl, and R. Lipowsky, Europhys. Lett. **53**, 618 (2001).
[26] P. Lenz, C. Bechinger, C. Schafle, P. Leiderer, and R. Lipowsky, ACS J. Surf. Coll. **17**, 7814 (2001).
[27] S. Nath, P. Nealey, and J.J. de Pablo, J. Chem. Phys. **110**, 7483 (1999).
[28] L.J. Douglas Frink and A.G. Salinger, J. Chem. Phys. **110**, 5969 (1999).
[29] W. Koch, S. Dietrich, and M. Napiórkowski, Phys. Rev. E **51**, 3300 (1995).
[30] M. Böltau, S. Walheim, J. Mlynek, G. Krausch, and U. Steiner, Nature (London) **391**, 877 (1998).
[31] N. Rehse, C. Wang, M. Hund, M. Geoghegan, R. Magerle, and G. Krausch, Eur. Phys. J. E **60**, 69 (2001).

[32] A. Karim, J.F. Douglas, B.P. Lee, S.C. Glotzer, J.A. Rogers, R.J. Jackman, E.J. Amis, and G.M. Whitesides, Phys. Rev. E **57**, R6273 (1998).

[33] L. Rockford, Y. Liu, P. Mansky, T.P. Russell, M. Yoor and S.G.J. Mochrie Phys. Rev. Lett. **82**, 2602 (1999).

[34] By convex interfaces we mean the convex shape of the liquid-vapor interface. In the case of a single interface, it is described by a concave function while convex bridgelike configuration is desribed by two functions: a convex and a concave one.

[35] A.J. Jin and M.E. Fisher, Phys. Rev. B **47**, 7365 (1993).

[36] Note that neglecting terms proportional to $\sim \tau^2$ in the analyzed expressions is consistent with the approximate form of the effective potential, Eq. (10), used in our analysis. It was shown within the Landau-Ginzburg-Wilson theory that the coefficient b in V contains—in addition to a constant—also a term proportional to τ^2 (see Ref. [35]). This term has been neglected in the form of V used in this work.